The Pennsylvania State University

The Graduate School

CONDUCTIVE SELF-HEALABLE BIOCOMPOSITES BASED ON PROTEIN MEDIATED SELF-ASSEMBLY OF PEDOT: PSS

A Thesis in

Engineering Science and Mechanics

by

Yusuke Kikuchi

© 2020 Yusuke Kikuchi

Submitted in Partial Fulfillment
of the Requirements
for the Degree of

Master of Science

May 2020

The thesis of Yusuke Kikuchi was reviewed and approved by the following:

Melik C. Demirel
Professor of Engineering Science and Mechanics
Thesis Adviser

Sahin K. Ozdemir
Associate Professor of Engineering Science and Mechanics

Judith Todd
Professor of Engineering Science and Mechanics
Head of the Department of Engineering Science and Mechanics

ABSTRACT

Abstract is adopted from Kikuchi et al., ACS Appl. Bio Mater. (accepted)

Composites of conducting polymers offer a broad spectrum of materials for interfacing electronic devices with biological systems. Particularly, material systems based on poly(styrenesulfonate) doped poly(3,4-ethylenedioxythiophene) (PEDOT: PSS) have found applications in many bioelectronic devices as biosensitive transistors, controlled drug delivery media, strain, temperature, and humidity sensors. The biocompatibility, intercoupled electronic and ionic conductivity, air stable electrical properties render PEDOT: PSS based material systems indispensable for bioelectronics. However, these materials are commonly used in thin film form since freestanding films of pristine PEDOT: PSS are considered mechanically brittle compared to biological tissues, and unlike biological systems these conductive films cannot restore/heal their physical properties after excessive mechanical deformation.

This thesis shows highly conductive biocomposites of PEDOT: PSS and tandem repeat proteins with the ability to self-heal once plasticized via water. The tandem repeat proteins acquired from squid ring teeth (SRT) induce structural effects on PEDOT:PSS including improved crystallinity and formation of fibrous network structures. These structural effects lead to electrical conductivity values reaching 120 S/cm for biocomposites with SRT protein concentrations below 20 wt. %, which exceeds conductivity of pristine PEDOT:PSS (~100 S/cm). More importantly, tandem proteins facilitate consistent self-healing of freestanding biocomposites with SRT protein concentrations beyond 40 wt. %. These robust biocomposites with high electrical conductivity and the ability to self-heal can find applications in numerous soft electronic systems spanning from implantable, transient, epidermal electronics to electronic textiles.

TABLE OF CONTENTS

LIST OF FIGURES

ACKNOWLEDGEMENTS

First, I express my deep gratitude to my Adviser, Dr. Melik C. Demirel for the guidance, motivation, and financial support for my thesis. I was very fortunate to work closely with adviser. I would like to thank my MS dissertation committee members, Dr. Sahin K. Ozdemir and for extensive personal and professional guidance and feedback for this thesis work. This complex interdisciplinary work would not have been possible without guidance from all my advisers and committee members from different fields of study.

Second, I am grateful to all of collaborators with whom I have had the pleasure to work during thesis work Dr. Benjamin D. Allen, Dr. Abdon Pena-Francesch, Dr. Natalia Domeradzka,, Dr. Mert Vural, Robert Shreiner, Benjamin Barbu, Joan Bars, Sezin Sayin, and Chloe Skidmore.

This thesis is supported partially by the Army Research Office (Grant no. W911NF-16-1-0019), the Huck Endowment, and the Pennsylvania State University internal funds.

Chapter 1

Introduction

Chapter 1 is adopted from Kikuchi et al., ACS Appl. Bio Mater. (accepted)

Implementation of electronic materials into biological systems holds great potential considering the recent developments in implantable, transient, epidermal electronics, and wearable bioelectronic systems devised for diagnostic medicine. However, the pace of advances in electronics employed for biomedicine suffers greatly from the mismatch between the mechanical properties of biological tissues, and electronic materials, particularly conductors. Hybrid/composite materials of soft polymers and conductive additives offers a variety of new possibilities that can address this problem [1–6]. Inorganic conductive additives are effective to establish composites with high electrical conductivity, yet the interface between brittle inorganic additives and soft polymer matrices engender additional problems like stiffening which elevates elastic modulus [5–8]. Blends of organic conductive fillers and soft polymers form more coherent mixtures and generate softer materials compared to composites with inorganic fillers [9–18]. More importantly, organic conductive additives can offer additional qualities like intercoupled electronic and ionic conductivity, which is essential for bioelectronic systems employed in diagnostic tools [19– 21] and drug delivery systems [22–24]. In particular, composites of poly(3,4-ethylenedioxythiophene) poly(styrenesulfonate) (PEDOT: PSS) are commonly used in soft electronic devices developed for biomedical applications, because of the unique transport properties and biocompatibility of this conjugated polymer blend. PEDOT: PSS is mostly used in thin film or composite form, since it is intrinsically brittle and prone to dissolution and degradation under physiological conditions [25,26].

One way to ensure biocompatibility of the conductive composites is matching PEDOT: PSS with biopolymers [27–31]. Biopolymers have been tested as stabilizers to replace PSS, but these blends exhibit significantly inferior electrical conductivity compared to PSS stabilized PEDOT [32–36]. The focus of the recent studies shifted towards blends of PEDOT: PSS and biopolymers including polysaccharides (cellulose, gellan and guar gum),[34–37] proteins (collagen, silk, heparin)[31,38–41] and DNA [33,42]. Biopolymers interact with PEDOT: PSS and prevent dissolution and degradation of conductive polymer, while sustaining biocompatibility of the composite material. The most significant challenge in biopolymer blends of PEDOT: PSS resides in the limited electrical conductivity of the resultant composites. Defined by the laws of percolation, electrical conductivity of the biocomposites decreases exponentially with increasing concentration of biopolymers [14,15]. However, biopolymers with the ability to influence the structure of PEDOT: PSS can extend the limits of percolation that impedes the electrical conductivity of the biocomposites.

Hydrogen bonding synthetic additives like ethylene glycol and polyethylene glycol are known to screen charge interactions between PSS ions and PEDOT crystals by facilitating hydrogen bonding with PSS ions [43–45] This effect drives a structural change in PEDOT:PSS system and improves electrical conductivity [43,44] Similarly, hydrogen bonding proteins with specific amino acid sequence engender constructive structural effects on conjugated polymers, which include but not limited to improved crystallinity and alignment of crystallites.46–48 These structural effects lead to biocomposites with electrical conductivity values extending beyond the limits of percolation [46–48] In addition it is possible to incorporate additional qualities like material strength and self-healing to conductive biocomposites via employing structural proteins [49–52].

Natural or biosynthethic production of structural proteins (e.g., silk, collagen, resilin, elastin, squid ring teeth protein) with repetitive polypeptides that comprise one or more tandem copies of a single unit have been an interest for the last couple of decades [52–54]. Their molecular structure provides a rich architecture that can micro-phase-separate to form periodic nanostructures (e.g., lamellar and cylindrical repeating phases, triple helix) with enhanced physicochemical properties that often exceed those of conventional synthetic polymers [52–54]. However, the studies focused on their utility in composite systems are rather new. [48,55,56]

Chapter 2 Experimental approach

Part of Chapter 2 is adopted from Kikuchi et al., ACS Appl. Bio Mater (accepted). This chapter includes the experimental setups of this thesis.

Fabrication of biocomposites:

The northern shortfin squids (Illex illecebrosus) originating from Cape Cod (USA) are purchased from (). Squid ring teeths (SRTs) are removed mechanically from suction cups. Extracted SRT are soaked in deionized (DI) water overnight to remove impurities. Wet SRTs were dried in vacuum desiccator. Dry SRTs are dissolved in anhydrous dimethylsulfoxide (DMSO) (Sigma-Aldrich Co. LLC., USA) at 70 ˚C. SRT solutions are centrifuged for 5 minutes at 10000rpm (Nanosep ®100K) to aggregate remaining impurities and undissolved proteins.

Dry pellets of PEDOT: PSS (Orgacon DRY) purchased from Sigma-Aldrich Co. LLC., USA are dissolved in DMSO to generate solutions with a final concentration of 15 mg/ml. To achieve homogeneous solutions the solutions are tip sonicated (60 W, for 5 mins, Fisherbrand 120W tip sonicator) for 5 minutes then continuously stirred prior to composite processing. SRT solutions with various concentrations are mixed with PEDOT: PSS solutions to generate composite solutions with desired compositions. The mixed solutions are constantly stirred prior to composite processing. The composite solutions are cast into PDMS molds with Teflon substrate to form desired shape.

Characterization:

The wide angle X-ray scattering experiments are performed by using an inhouse SAXS/WAXS laboratory system (Xeuss 2.0 HR, Xenocs, France) equipped with a microfocus sealed tube (copper) with X-ray wavelength of 1.54 Å (50 kV, 0.6 mA) and a Pilatus3 R200K detector with a sample to detector distance of approximately 0.165 m. The scattering experiments are collected under vacuum at room temperature and integrated over a tilted circle profile to convert 2D images into one-dimensional scattering patterns of scattering intensity I(q) (in arbitrary units) versus degrees 2theta.

The surface morphology of PEDOT: PSS/SRT biocomposites are characterized using Scanning Electron Microscopy (SEM) (FEI Nova NanoSEM 450, Philips XL30). SEM images are acquired with an accelerating voltage of 5 kV. EDS of biocomposites are collected via Philips XL30 with an integrated EDAX system.

Fourier transform infrared (FTIR) spectra are collected (Thermo Scientific Nicolet 6700 FT-IR) under attenuated total reflection (diamond crystal) mode using Happ-Genzel apodization with 4 cm−1 resolutions from wavenumber 400 to 4000 cm−1. For each spectrum, 256 scans are co-added. Dynamic light scattering measurements are performed on composite solutions prior to casting. Colloidal particle sizes generated by SRT and PEDOT: PSS in composite solutions are collected by using Zetasizer Nano ZS. Highly concentrated composite solutions are diluted to %0.1 v/v to acquire accurate DLS data.

The electrical conductivity of biocomposite films are carried out using a four-point probe apparatus (2 mm inter-probe distance) connected to a sourcemeter (Keithley 2400). Light Emitting Diode (LED) circuit is fabricated with a biocomposite as electrode. The luminosity of LED is monitored prior and after self-healing of biocomposite. The resistance of the biocomposite electrode of the LED circuit before and after self-healing is monitored using multimeter.

Chapter 3 Results and discussions

Part of Chapter 2 is adopted from Kikuchi et al., Kikuchi et al., ACS Appl. Bio Mater (accepted).

Self-healing conductive biocomposites are prepared via solution processing methods (Figure 1a). First, SRT proteins are extracted from the tentacles of northern shortfin squids (Illex illecebrosus) suction cups and purified according to the protocols published earlier.51,58 These soft biopolymer cups consist of 15-55kDa polypeptides of highly repetitive structural proteins with a segmented copolymer architecture (Figure 1b) [52–54]. Proteins with shorter amino acid sequences generate a thermoplastic protein, while proteins with longer sequences result in a material with extraordinary elasticity and robustness [52,59]. The effective combination of these sequences leads to a protein with novel viscoelastic properties in dry and humidified state.60 Purified SRT proteins are later dissolved in dimethylsulfoxide (DMSO) at various concentrations (Figure 1c). The proper dissolution of proteins in solution and increase in protein concentration is verified using infrared spectroscopy (Figure 2). Once poured in polytetrafluoroethylene (PTFE) molds, these solutions form flexible, transparent SRT films, that are potent adhesives under water (Figure 1c).51 Following the preparation of SRT solutions, dry pellets of PEDOT: PSS are dispersed in DMSO using a separate vial. SRT and PEDOT: PSS solutions are then slowly mixed to achieve the final solution (Figure 1d). Mixed solutions are cast on PTFE molds in a desired shape to fabricate freestanding films of conductive biocomposites (Figure 1d). The cast biocomposites are placed in a vacuum desiccator overnight to remove excess DMSO and facilitate formation of void-free and uniform biocomposite films. These freestanding biocomposites maintain their shape and properties under physiological conditions, dissimilar to pristine PEDOT: PSS, which bleeds excess PSS after being exposed to physiological conditions (Figure 3).

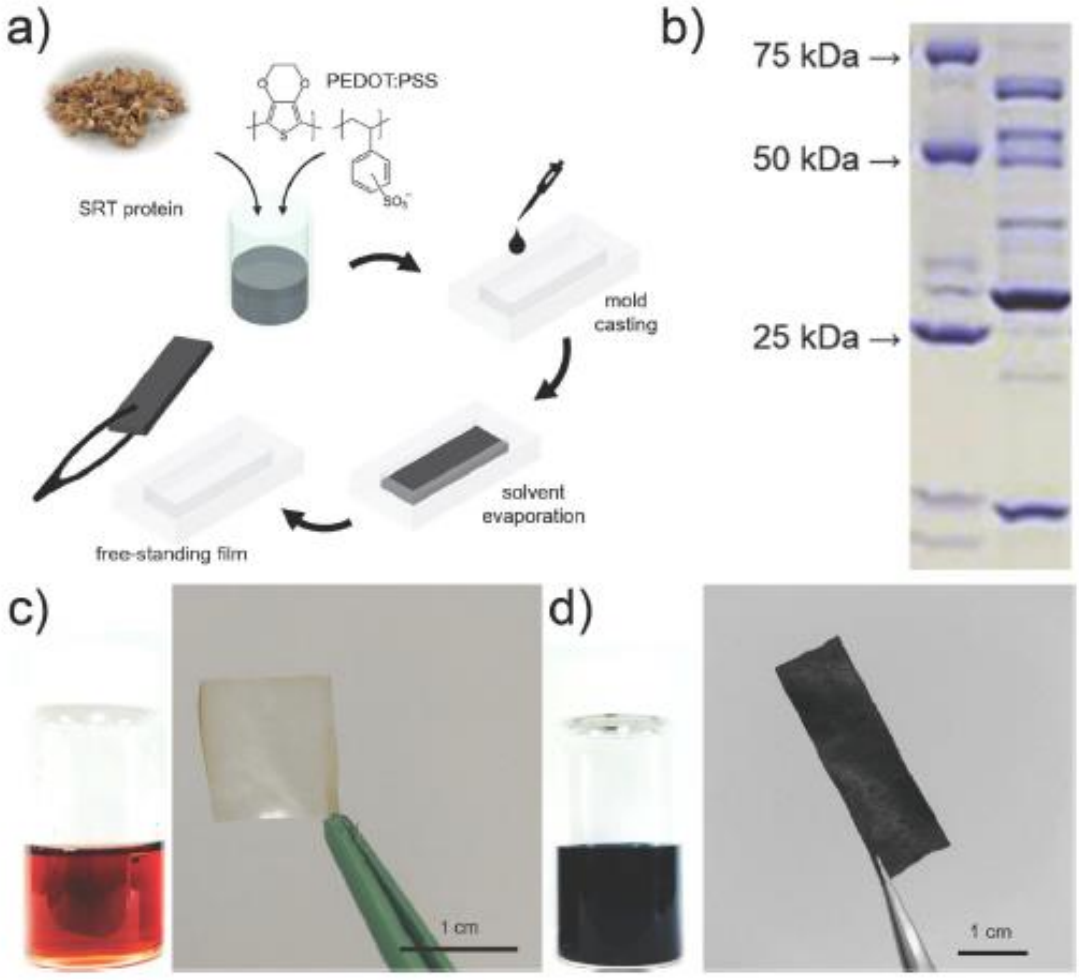

Figure 1 a) Solution processed fabrication of SRT/PEDOT: PSS conductive biocomposites. b) SDS/Page gel chromatography identifying molecular weight of SRT proteins extracted from Illex illecebrosus suction cups. c) Images of SRT/DMSO solutions and SRT films prepared from these solutions. d) Images of SRT/PEDOT: PSS/DMSO solutions and conductive biocomposite films prepared from these solutions.

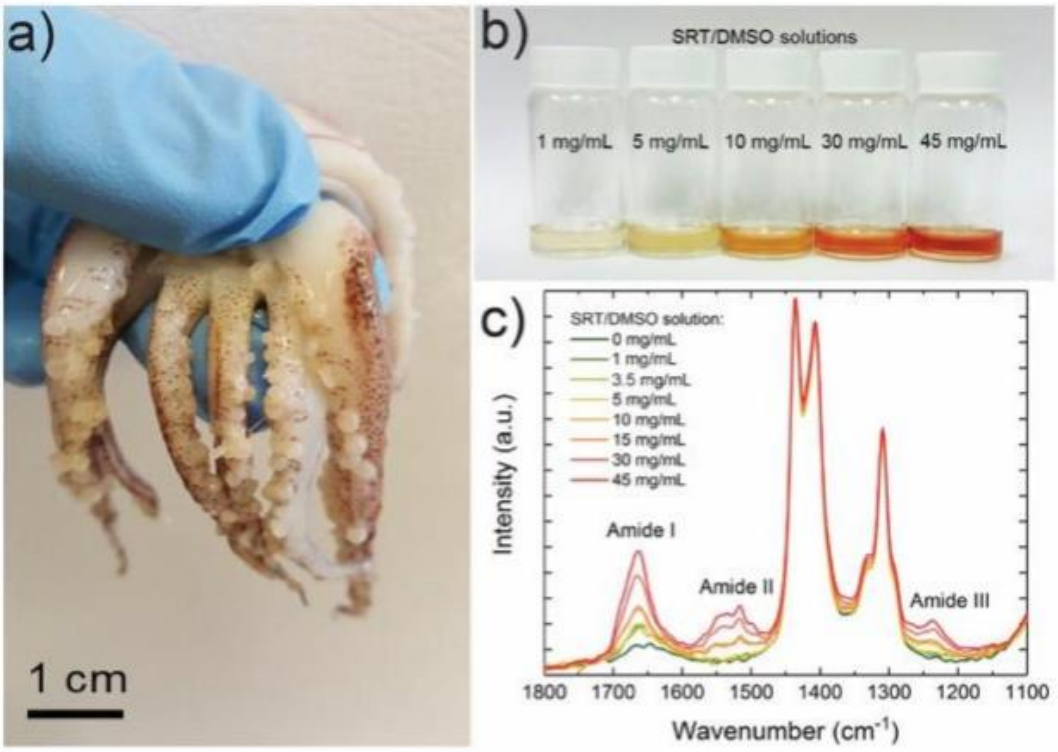

Figure 2: a) Picture of Loligo Pelei, b) the different concentration of SRT/DMSO solutions, and c) IR data of each solutions

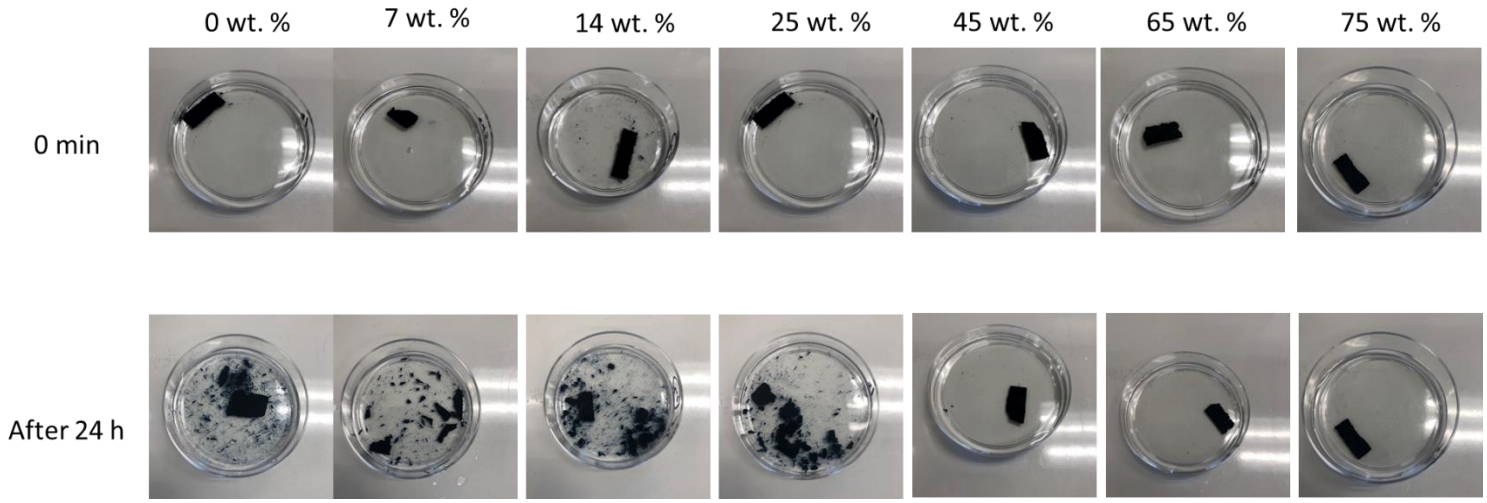

Figure 3: Images of degradation for PEDOT: PSS and PEDOT: PSS/SRT biocomposite films immersed in water for 24h

The initial structural characterization of conductive biocomposites with different protein concentrations is performed using high resolution simultaneous small-angle X-ray scattering (SAXS) and wide-angle X-Ray scattering (WAXS) measurements. Samples composed of pristine PEDOT: PSS films exhibit a solitary peak representing (100) orientation of PEDOT crystals located at 2θ=4.72° (Figure 4a). This corresponds to an interplanar spacing of 18.7 Å between lamellar PEDOT crystals (Figure 4a) [50,61]. Pristine PEDOT: PSS films cast from DMSO feature two more peaks centered at 2θ=18° and 2θ=26°, which represents an amorphous halo of PSS chains, and a planar ring stacking distance (010) of PEDOT crystals (Figure 4a). This X-ray diffraction (XRD) data is consistent with previously reported structural characteristics of PEDOT: PSS films cast from DMSO solutions [62]. Biocomposites consisting of SRT and PEDOT:PSS exhibit additional diffraction peaks mostly originating from the structural features of SRT (Figure 4a) [50] The diffraction peaks originating from SRT proteins located at 2θ=9.5°, 2θ=19.2°, and 2θ=24° correspond to (100) reflections of beta (β) sheets, amorphous halo of proteins, and (002) reflections of β sheets, respectively (Figure 4a). These reflections become more pronounced with increasing concentration of SRT proteins in biocomposites (Figure 4a). Interestingly at SRT concentrations exceeding 40wt. % (100) reflections of PEDOT crystals split into two distinct peaks located at 2θ=3.8° and 2θ=5.1°, which is more analogous to the structure of PEDOT crystals in films cast from aqueous PEDOT:PSS solutions (Figure 4b) [57]. However, the most significant impact of SRT on the structure of PEDOT: PSS occurs at protein concentrations lower than 25wt. % (Figure 4c). The PEDOT crystal peaks at (100) become visibly sharper and higher in diffracted intensity with gradual increase in SRT concentration (Figure 4d). The PEDOT crystal size quantified using Scherrer formula63 for pristine PEDOT: PSS films and biocomposites composed of 25wt. % SRT are 2.6 nm and 3.8 nm, respectively. The increase in diffracted beam intensity with increasing SRT concentration also indicates an improvement in crystallinity of PEDOT in biocomposites (Figure 4d). The improved crystallinity and increased crystal size are prominent structural effects that are

known to improve charge transport and electrical conductivity in PEDOT: PSS systems [43,44,57]. To further evaluate the structure of the composites prepared using DMSO solutions of SRT and PEDOT: PSS, we performed dynamic light scattering (DLS) experiments on DMSO/SRT and DMSO/PEDOT: PSS solutions (Figure 5). DLS measurements indicate that SRT assembles into two distinct forms of colloids (Figure 5). A significant population of the SRT colloids formed in DMSO solutions have a size distribution centered at 600 nm (Figure 5). SRT also forms smaller colloids with a size distribution centered at 100 nm in DMSO solutions (Figure 4f). These size distributions agree well with the colloidal size distributions observed for SRT proteins dissolved in aqueous acetic acid solutions.64 The sharp scattering peak centered at 5 nm observed in DLS data of DMSO/SRT solutions originate from the undissolved crystalline beta sheets formed by SRT (Figure 5), which was also observed in DLS data of aqueous acetic acid solutions of SRT [64].

The DLS measurements of DMSO/PEDOT: PSS solutions exhibit a single colloidal size distribution centered at 25 nm (Figure 4e, 4f). This observation is consistent with DLS measurements performed on aqueous PEDOT: PSS solutions prepared using various sources of PEDOT: PSS (Clevios PH1000, Orgacon from Agfa Chemicals).65–67 This data suggests that DMSO have minimal influence on the size of the PEDOT: PSS colloids. The DLS analysis of solutions used to cast PEDOT: PSS/SRT biocomposites exhibit several characteristic size distributions corresponds to PEDOT: PSS and SRT. The characteristic size of PEDOT: PSS colloids centered at 25 nm shifts towards larger dimensions in the DLS spectra of biocomposite solutions (Figure 4f). In complement to this observation, the characteristic colloidal size distribution observed for both DMSO and acetic acid solutions of SRT with an average colloid dimension of 100 nm disappears for biocomposite solutions (Figure 4f). This suggests that SRT molecules are interacting with PSS and affecting structure of PEDOT: PSS colloids, hence increasing the PEDOT: PSS colloid size instead of forming SRT colloids in DMSO. This observation is in concert with the structural changes observed during XRD analysis, which

highlights an increase in the crystal size and crystallinity of the PEDOT that likely benefits from the increased size of PEDOT: PSS colloids. Biocomposite solutions sustains the large colloids of SRT with an average diameter of 600 nm, which originates from the excess SRT molecules that cannot interact with PSS (Figure 4e). Biocomposite solutions with SRT concentrations exceeding 65wt. % demonstrates a size distribution centered at 5 nm (Figure 4f), which corresponds to β sheets that are also present in DLS spectra of SRT/DMSO solutions (Figure 5).

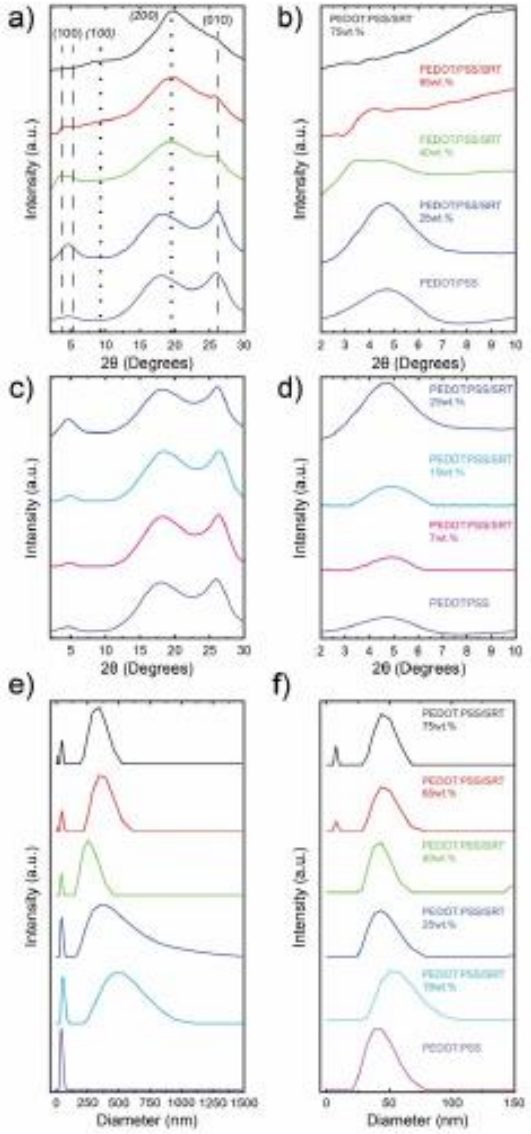

Figure 4: a) XRD spectra for pristine PEDOT:PSS and PEDOT:PSS/SRT biocomposites with different SRT (25wt. %, 40wt. %, 65wt. %, 75wt. %) concentrations (italic planar orientations represent SRT). b) a) XRD spectra for pristine PEDOT:PSS and PEDOT:PSS/SRT composites with different SRT concentrations focused on smaller angles (2θ=2°-10°). c) XRD spectra for pristine PEDOT:PSS and PEDOT:PSS/SRT biocomposites with various SRT (7wt. %, 19wt. %, 25wt. %) concentrations. d) XRD spectra for pristine PEDOT:PSS and PEDOT:PSS/SRT biocomposites with various SRT (7wt. %, 19wt. %, 25wt. %) concentrations focused on smaller angles (2θ=2°-10°). e) DLS spectra of PEDOT:PSS and PEDOT:PSS/SRT biocomposites with different SRT concentrations (19wt. %, 25wt. %, 40wt. %, 65wt. %, 75wt. %). f) DLS spectra of PEDOT:PSS and PEDOT:PSS/SRT biocomposites with different SRT concentrations (19wt. %, 25wt. %, 40wt. %, 65wt. %, 75wt. %) focused on smaller dimensions (0 nm-150 nm).

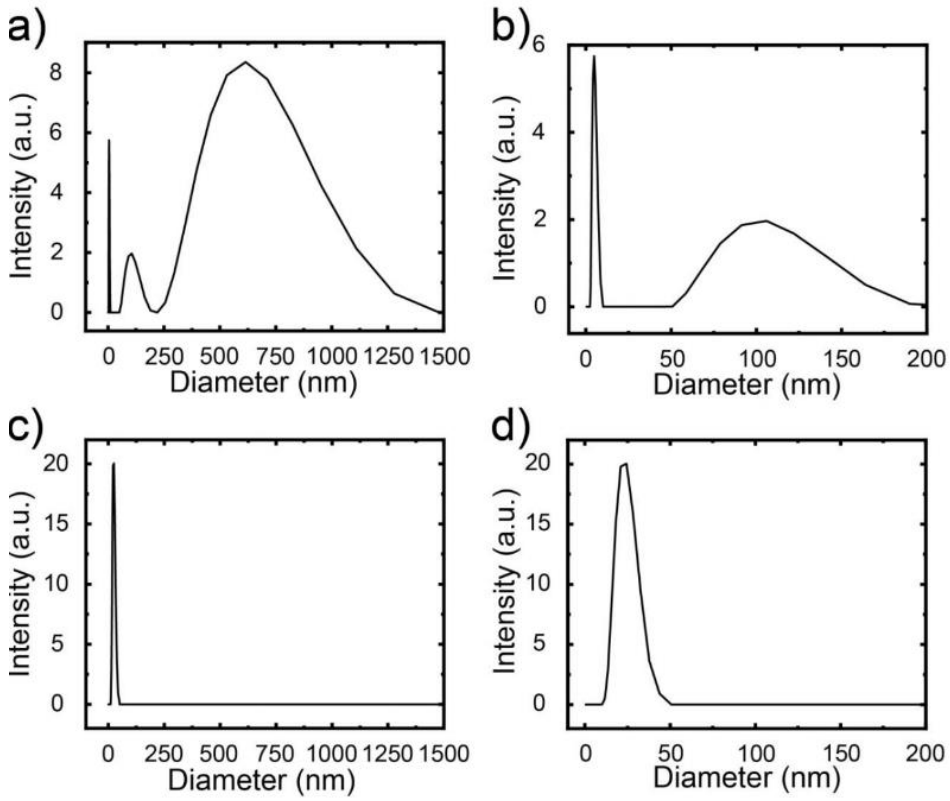

Figure 5: a) Dynamic Light Scattering (DLS) spectrum of SRT/DMSO solution. b) DLS spectrum of SRT/DMSO solution focused on smaller dimensions (0 nm-150 nm). c) Dynamic Light Scattering (DLS) spectrum of PEDOT: PSS/DMSO solution. b) DLS spectrum of PEDOT: PSS/DMSO solution focused on smaller dimensions (0 nm-150 nm)

The changes in microstructure of PEDOT: PSS originating from the presence of SRT have significant impact on electrical properties. However, the presence of SRT proteins can lead to structural changes in microscale, which can also affect the electrical transport properties of PEDOT: PSS drastically. To evaluate microscale changes in the structure of the composites, we performed electron microscopy studies on pristine PEDOT: PSS and biocomposites consisting of PEDOT: PSS and SRT proteins (Figure 6). Pristine PEDOT: PSS films cast from DMSO solutions of dry PEDOT: PSS pellets exhibit uniform films with no distinct structural features (Figure 6a). The addition of SRT initiates formation of fibrous structures for films with SRT concentrations reaching 25wt. % (Figure 6a-6f). For composites with SRT concentrations exceeding 25wt. %, the fiber density gradually decreases, and fiber morphology becomes obscure for biocomposites with SRT concentration of 40wt. % (Figure 6g, 6h). Formation of nanofibers is not uncharacteristic for PEDOT:PSS systems with the help of additives or treatments, however the size of these fibers do not exceed 50 nm.[25,57] Biocomposites of SRT and PEDOT:PSS form fibers with diameters reaching several hundred nanometers ($d_{average}=700 \pm 200$ nm) via self-assembly, which has not been observed for any material system involving SRT and PEDOT:PSS. Biocomposites with SRT concentrations over 50 wt. % demonstrate non-conductive aggregates of proteins (Figure 6i-6l). The compositions of these aggregates are also confirmed using energy dispersive X-ray spectroscopy (EDS) (Figure 7). The structural changes initiated by SRT proteins in microscale and nanoscale concur with each other and indicate that SRT proteins promote structures that can help improve electronic transport in biocomposites for concentrations up to 25wt. % SRT. Beyond this concentration the excess SRT in biocomposites act like a polymer matrix in this composite system and contribute to the structure as mechanical support.

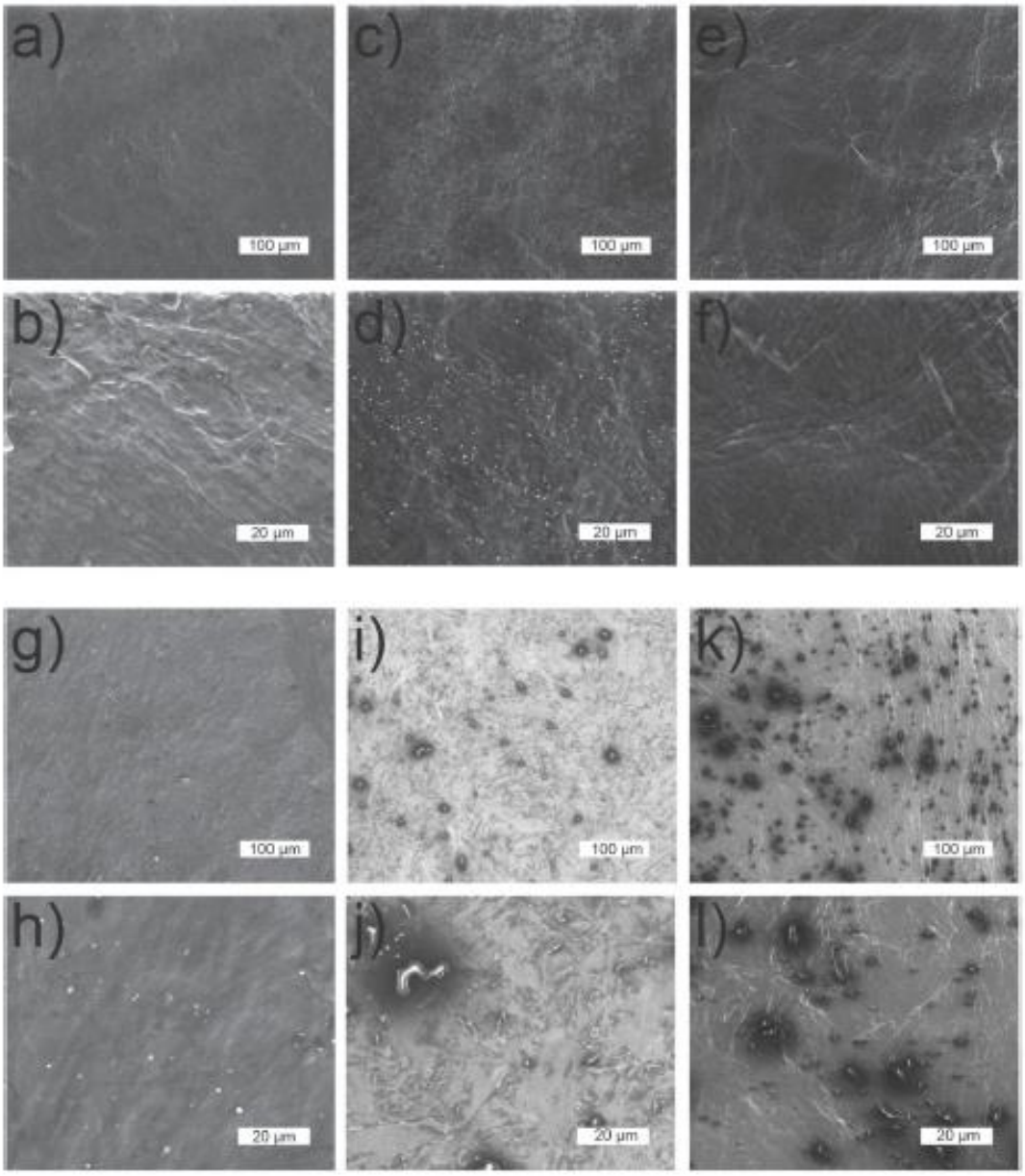

Figure 6: Scanning electron microscope (SEM) images of a, b) PEDOT: PSS films cast from DMSO. SEM images of conductive biocomposites consisting of c, d) 7wt. % SRT, e, f) 19wt. % SRT, g, h) 25wt. % SRT, i, j) 65wt. % SRT, k, l) 75wt. % SRT and PEDOT: PSS.

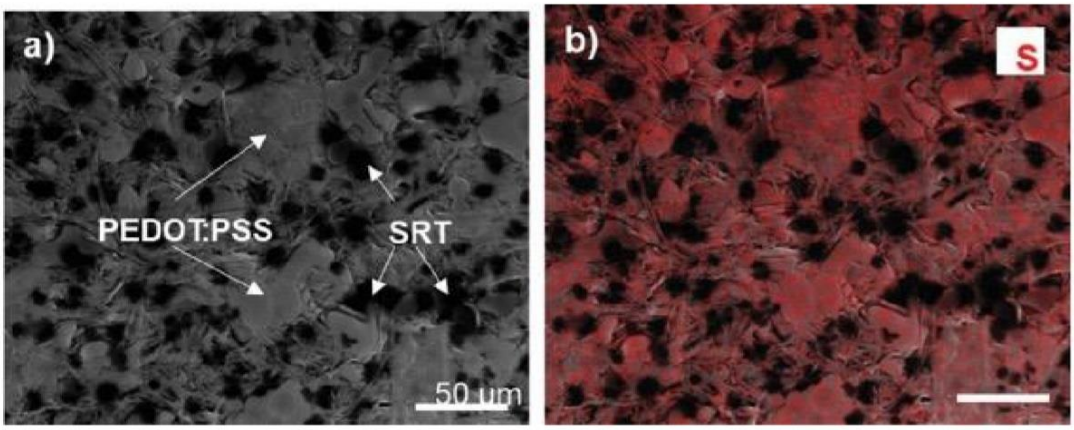

Figure 7: EDS data of the composite film

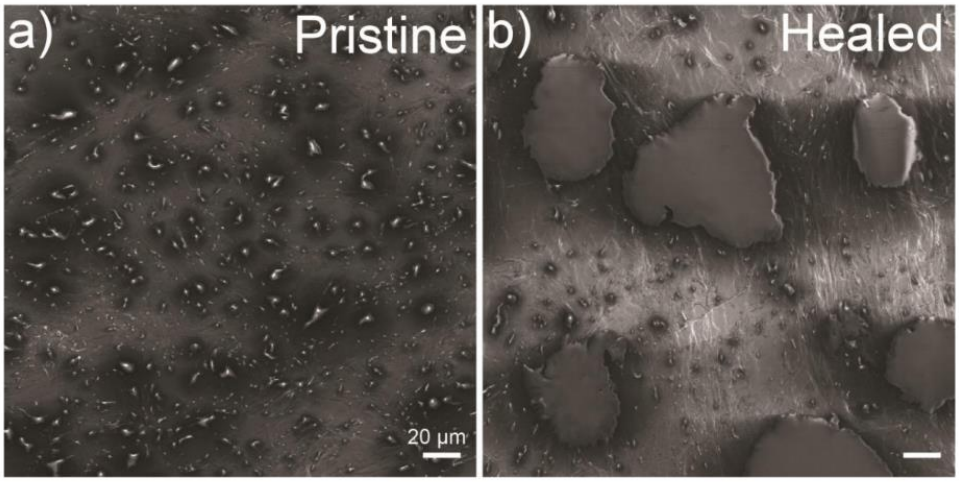

Figure 8; SEM image of PEDOT: PSS/SRT biocomposite film (65 wt. % SRT) a) prior and b) after self-healing.

The influence of structural changes on the electrical properties and the ability to heal sustained damage for conductive biocomposites are evaluated by performing 4-point probe experiments on biocomposites before and after cutting the sample into two pieces (Figure 9a-9b). The electrical conductivity of biocomposites composed of different SRT concentrations are in concert with the structural changes observed in conductive biocomposites with altering SRT concentrations (Figure 9b). In contradiction with percolation theory, the electrical conductivity of biocomposites increase, with increasing SRT concentration up to a threshold concentration of 20 wt. % SRT. Improved crystallinity of PEDOT and formation of fibrous network structures are known to generate pathways with higher mobility for electron transport [57,68]. Low volumetric concentrations of SRT induce similar changes in microstructure of PEDOT: PSS, as demonstrated during the structural characterization of biocomposites of SRT and PEDOT: PSS (Figure 4, Figure 6). The divergence of the conductivity values from the conventional percolation theory possibly originates from these structural effects for composites with SRT concentrations below 20 wt. %. Beyond this concentration percolative effects begin to dominate over constructive structural effects originating from the interactions between SRT and PEDOT: PSS. At the concentration threshold biocomposites exhibit electrical conductivity values reaching 120 S/cm (Figure 9b).

Conductive organic biocomposites are tested for their ability to recover electrical properties after repetitive incisions. The biocomposites are cut in the middle and remerged using heat and pressure under aqueous conditions to perform mechanical and electrical recovery (Figure 9a). After healing protocol, the electrical conductivity values of the biocomposites are remeasured to quantify the extent of recovery in electrical properties (Figure 9b). It is possible to infer that biocomposites requires excess SRT matrix as a mechanical support to facilitate complete recovery from incision damage. At SRT concentrations above 40 wt. % SRT, electrical properties of the conductive biocomposites are completely restored after healing. The mechanism behind this recovery can be explained by the underwater adhesion properties of SRT [51,58] and the interaction between SRT

chains and PSS [43,44]. The SRT proteins soften at temperatures exceeding 70°C at the presence of water, which acts as a plasticizer for proteins [58]. SRT proteins interacting with PSS ions form an interface with PEDOT: PSS system, and excess proteins connect different PEDOT: PSS systems via hydrogen bonding (Figure 9c, Figure 8). After incision, proteins can reform the hydrogen bonds severed during the mechanical damage while plasticized at aqueous conditions and healing temperature (70°C). The biocomposites that exhibit 50 S/cm electrical conductivity can sustain their electrical properties after several incisions. The self-healing aspect of biocomposites is utilized in a simple light emitting diode (LED) circuit connected using conductive biocomposites (Figure 9d). The luminosity of the light remains unaltered after cutting and healing the biocomposite electrode (Figure 6d). In addition, the resistance of the biocomposite electrode remains unchanged after the cutting and healing protocol.

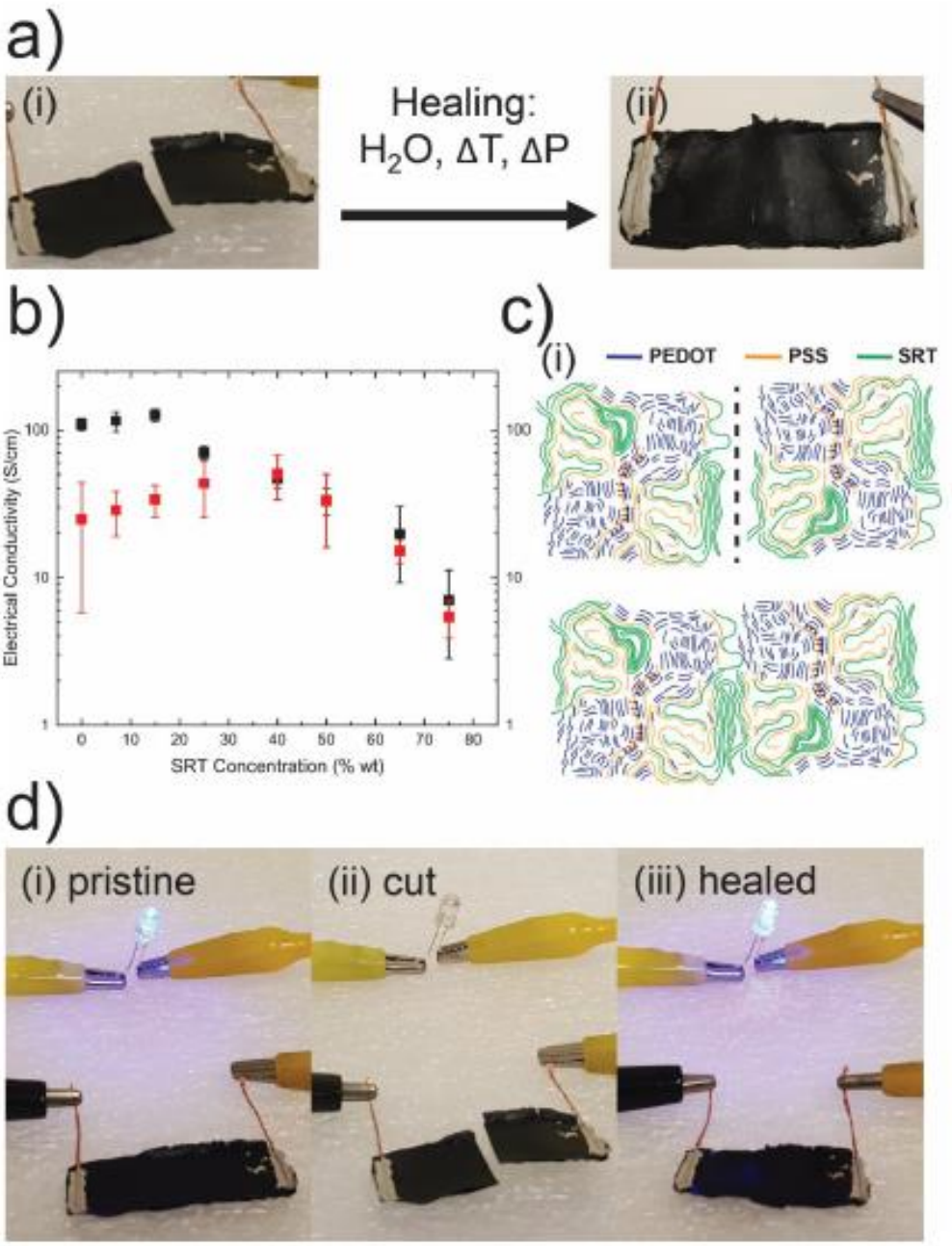

Figure 9 : a) Images of conductive biocomposites (composition) i) after incision and ii) healing process. b) Electrical properties of conductive biocomposites prior (black), after (red) cutting and healing process. c) Schematic illustration of healing process of conductive biocomposites after incision. d) Images of LED circuit operating i) prior to cutting, ii) after cutting, and iii) after the healing process.

Chapter 4 Conclusion

Part of Chapter 4 is adopted from Kikuchi et al., ACS Appl. Bio Mater. (accepted)

In summary, we demonstrated composites of structural protein SRT and PEDOT: PSS that form fibrous self-healing conductors via self-assembly. These composites exhibit extraordinary electrical properties facilitated by the specific interactions between SRT and PSS chains. These interactions lead to improved PEDOT crystallinity and formation of a fibrous network, which helps these biocomposites to attain electrical conductivity values higher than pristine PEDOT: PSS films. SRT/PEDOT: PSS biocomposites can reach conductivity values of 120 S/cm, while PEDOT: PSS films cast from DMSO exhibit conductivity values of 100 S/cm. In addition, excess SRT facilitates the ability to self-heal in these conductive biocomposites. Conductive biocomposites with electrical conductivity values of 50 S/cm can be cut and healed for multiple cycles yet sustain their electrical properties after healing process. One particularly appealing aspect of conductive self-healing biocomposites with exceptional electrical properties is their prospect in emerging soft electronics applications spanning from wearable electronics to diagnostic biomedicine

Bibliography

(1) Sekitani, T.; Noguchi, Y.; Hata, K.; Fukushima, T.; Aida, T.; Someya, T. A Rubberlike Stretchable Active Matrix Using Elastic Conductors. Science (80-.). 2008, 321 (5895), 1468 LP – 1472. https://doi.org/10.1126/science.1160309.

(2) Lipomi, D. J.; Vosgueritchian, M.; Tee, B. C.-K.; Hellstrom, S. L.; Lee, J. A.; Fox, C. H.; Bao, Z. Skin-like Pressure and Strain Sensors Based on Transparent Elastic Films of Carbon Nanotubes. Nat. Nanotechnol. 2011, 6 (12), 788–792. https://doi.org/10.1038/nnano.2011.184.

(3) Kim, K. H.; Vural, M.; Islam, M. F. Single-Walled Carbon Nanotube Aerogel-Based Elastic Conductors. Adv. Mater. 2011, 23 (25), 2865–2869. https://doi.org/10.1002/adma.201100310.

(4) Kim, Y.; Zhu, J.; Yeom, B.; Di Prima, M.; Su, X.; Kim, J.-G.; Yoo, S. J.; Uher, C.; Kotov, N. A. Stretchable Nanoparticle Conductors with Self-Organized Conductive Pathways. Nature 2013, 500, 59. (

(5) Matsuhisa, N.; Inoue, D.; Zalar, P.; Jin, H.; Matsuba, Y.; Itoh, A.; Yokota, T.; Hashizume, D.; Someya, T. Printable Elastic Conductors by in Situ Formation of Silver Nanoparticles from Silver Flakes. Nat. Mater. 2017, 16, 834.

(6) Choi, S.; Han, S. I.; Jung, D.; Hwang, H. J.; Lim, C.; Bae, S.; Park, O. K.; Tschabrunn, C. M.; Lee, M.; Bae, S. Y.; et al. Highly Conductive, Stretchable and Biocompatible Ag–Au Core–Sheath Nanowire Composite for Wearable and Implantable Bioelectronics. Nat. Nanotechnol. 2018, 13 (11), 1048–1056. https://doi.org/10.1038/s41565-018-0226-8.

(7) Vural, M.; Behrens, A. M.; Ayyub, O. B.; Ayoub, J. J.; Kofinas, P. Sprayable Elastic Conductors Based on Block Copolymer Silver Nanoparticle Composites. ACS Nano 2015, 9 (1), 336–344. https://doi.org/10.1021/nn505306h

(8) Vural, M.; Behrens, A. M.; Hwang, W.; Ayoub, J. J.; Chasser, D.; Cresce, A. von W.; Ayyub, O. B.; Briber, R. M.; Kofinas, P. Spray-Processed Composites with High Conductivity and Elasticity. ACS Appl. Mater. Interfaces 2018, 10 (16), 13953–13962. https://doi.org/10.1021/acsami.8b00068.

(9) Seyedin, M. Z.; Razal, J. M.; Innis, P. C.; Wallace, G. G. Strain-Responsive Polyurethane/PEDOT:PSS Elastomeric Composite Fibers with High Electrical Conductivity. Adv. Funct. Mater. 2014, 24 (20), 2957–2966. https://doi.org/10.1002/adfm.201303905.

(10) Choong, C.-L.; Shim, M.-B.; Lee, B.-S.; Jeon, S.; Ko, D.-S.; Kang, T.-H.; Bae, J.; Lee, S. H.; Byun, K.-E.; Im, J.; et al. Highly Stretchable Resistive Pressure Sensors Using a Conductive Elastomeric Composite on a Micropyramid Array. Adv. Mater. 2014, 26 (21), 3451–3458. https://doi.org/10.1002/adma.201305182.

(11) Li, P.; Sun, K.; Ouyang, J. Stretchable and Conductive Polymer Films Prepared by Solution Blending. ACS Appl. Mater. Interfaces 2015, 7 (33), 18415–18423. https://doi.org/10.1021/acsami.5b04492.

(12) Kayser, L. V; Lipomi, D. J. Stretchable Conductive Polymers and Composites Based on PEDOT and PEDOT:PSS. Adv. Mater. 2019, 31 (10), 1806133. https://doi.org/10.1002/adma.201806133.

(13) Sasaki, M.; Karikkineth, B. C.; Nagamine, K.; Kaji, H.; Torimitsu, K.; Nishizawa, M. Highly Conductive Stretchable and Biocompatible Electrode–Hydrogel Hybrids for Advanced Tissue Engineering. Adv. Healthc. Mater. 2014, 3 (11), 1919–1927. https://doi.org/10.1002/adhm.201400209.

(14) Belaineh, D.; Andreasen, J. W.; Palisaitis, J.; Malti, A.; Håkansson, K.; Wågberg, L.; Crispin, X.; Engquist, I.; Berggren, M. Controlling the Organization of PEDOT:PSS on Cellulose Structures. ACS Appl. Polym. Mater. 2019, 1 (9), 2342–2351. https://doi.org/10.1021/acsapm.9b00444.

(15) Edberg, J.; Malti, A.; Granberg, H.; Hamedi, M. M.; Crispin, X.; Engquist, I.; Berggren, M. Electrochemical Circuits from ‘Cut and Stick’ PEDOT:PSS-Nanocellulose Composite. Flex. Print. Electron. 2017, 2 (4), 45010. https://doi.org/10.1088/2058-8585/aa8027.

(16) Inal, S.; Hama, A.; Ferro, M.; Pitsalidis, C.; Oziat, J.; Iandolo, D.; Pappa, A.-M.; Hadida, M.; Huerta, M.; Marchat, D.; et al. Conducting Polymer Scaffolds for Hosting and Monitoring 3D Cell Culture. Adv. Biosyst. 2017, 1 (6), 1700052. https://doi.org/10.1002/adbi.201700052.

(17) Malti, A.; Edberg, J.; Granberg, H.; Khan, Z. U.; Andreasen, J. W.; Liu, X.; Zhao, D.; Zhang, H.; Yao, Y.; Brill, J. W.; et al. An Organic Mixed Ion–Electron Conductor for Power Electronics. Adv. Sci. 2016, 3 (2), 1500305. https://doi.org/10.1002/advs.201500305.

(18) Pitsalidis, C.; Ferro, M. P.; Iandolo, D.; Tzounis, L.; Inal, S.; Owens, R. M. Transistor in a Tube: A Route to Three-Dimensional Bioelectronics. Sci. Adv. 2018, 4 (10), eaat4253. https://doi.org/10.1126/sciadv.aat4253.

(19) Mabeck, J. T.; Malliaras, G. G. Chemical and Biological Sensors Based on Organic ThinFilm Transistors. Anal. Bioanal. Chem. 2006, 384 (2), 343–353. https://doi.org/10.1007/s00216-005-3390-2.

(20) Khodagholy, D.; Doublet, T.; Quilichini, P.; Gurfinkel, M.; Leleux, P.; Ghestem, A.; Ismailova, E.; Hervé, T.; Sanaur, S.; Bernard, C.; et al. In Vivo Recordings of Brain Activity Using Organic Transistors. Nat. Commun. 2013, 4 (1), 1575. https://doi.org/10.1038/ncomms2573.

(21) Berggren, M.; Richter-Dahlfors, A. Organic Bioelectronics. Adv. Mater. 2007, 19 (20), 3201–3213. https://doi.org/10.1002/adma.200700419.

(22) Isaksson, J.; Kjäll, P.; Nilsson, D.; Robinson, N.; Berggren, M.; Richter-Dahlfors, A. Electronic Control of Ca2+ Signalling in Neuronal Cells Using an Organic Electronic Ion Pump. Nat. Mater. 2007, 6 (9), 673–679. https://doi.org/10.1038/nmat1963.

(23) Simon, D. T.; Kurup, S.; Larsson, K. C.; Hori, R.; Tybrandt, K.; Goiny, M.; Jager, E. W. H.; Berggren, M.; Canlon, B.; Richter-Dahlfors, A. Organic Electronics for Precise Delivery of Neurotransmitters to Modulate Mammalian Sensory Function. Nat. Mater. 2009, 8 (9), 742–746. https://doi.org/10.1038/nmat2494.

(24) Bernacka-Wojcik, I.; Huerta, M.; Tybrandt, K.; Karady, M.; Mulla, M. Y.; Poxson, D. J.; Gabrielsson, E. O.; Ljung, K.; Simon, D. T.; Berggren, M.; et al. Implantable Organic Electronic Ion Pump Enables ABA Hormone Delivery for Control of Stomata in an Intact Tobacco Plant. Small 2019, 0 (0), 1902189. https://doi.org/10.1002/smll.201902189.

(25) Lu, B.; Yuk, H.; Lin, S.; Jian, N.; Qu, K.; Xu, J.; Zhao, X. Pure PEDOT:PSS Hydrogels. Nat. Commun. 2019, 10 (1), 1043. https://doi.org/10.1038/s41467-019-09003-5.

(26) Ouyang, L.; Wei, B.; Kuo, C.; Pathak, S.; Farrell, B.; Martin, D. C. Enhanced PEDOT Adhesion on Solid Substrates with Electrografted P(EDOTNH₂). Sci. Adv. 2017, 3 (3), e1600448. https://doi.org/10.1126/sciadv.1600448.

(27) Tanaka, H.; Herland, A.; Lindgren, L. J.; Tsutsui, T.; Andersson, M. R. Enhanced Current Efficiency from Bio-Organic Light-Emitting Diodes Using Decorated Amyloid Fibrils with Conjugated Polymer. Nano Lett. 2008, 8 (9), 2858–2861. https://doi.org/10.1021/nl801510z.

(28) Tsukada, S.; Nakashima, H.; Torimitsu, K. Conductive Polymer Combined Silk Fiber Bundle for Bioelectrical Signal Recording. PLoS One 2012, 7 (4), e33689.

(29) Bongo, M.; Winther-Jensen, O.; Himmelberger, S.; Strakosas, X.; Ramuz, M.; Hama, A.; Stavrinidou, E.; Malliaras, G. G.; Salleo, A.; Winther-Jensen, B.; et al. PEDOT:Gelatin Composites Mediate Brain Endothelial Cell Adhesion. J. Mater. Chem. B 2013, 1 (31), 3860–3867. https://doi.org/10.1039/C3TB20374C.

(30) Pal, R. K.; Farghaly, A. A.; Wang, C.; Collinson, M. M.; Kundu, S. C.; Yadavalli, V. K. Conducting Polymer-Silk Biocomposites for Flexible and Biodegradable Electrochemical Sensors. Biosens. Bioelectron. 2016, 81, 294–302. https://doi.org/https://doi.org/10.1016/j.bios.2016.03.010.

(31) Bäcklund, F. G.; Elfwing, A.; Musumeci, C.; Ajjan, F.; Babenko, V.; Dzwolak, W.; Solin, N.; Inganäs, O. Conducting Microhelices from Self-Assembly of Protein Fibrils. Soft Matter 2017, 13 (25), 4412–4417. https://doi.org/10.1039/C7SM00068E.

(32) Thaning, E. M.; Asplund, M. L. M.; Nyberg, T. A.; Inganäs, O. W.; von Holst, H. Stability of Poly(3,4-Ethylene Dioxythiophene) Materials Intended for Implants. J. Biomed. Mater. Res. Part B Appl. Biomater. 2010, 93B (2), 407–415. https://doi.org/10.1002/jbm.b.31597.

(33) Ner, Y.; Invernale, M. A.; Grote, J. G.; Stuart, J. A.; Sotzing, G. A. Facile Chemical Synthesis of DNA-Doped PEDOT. Synth. Met. 2010, 160 (5), 351–353. https://doi.org/https://doi.org/10.1016/j.synthmet.2009.11.003.

(34) Lv, R.; Sun, Y.; Yu, F.; Zhang, H. Fabrication of Poly(3,4-Ethylenedioxythiophene)Polysaccharide Composites. J. Appl. Polym. Sci. 2012, 124 (1), 855–863. https://doi.org/10.1002/app.35117.
(35) del Agua, I.; Mantione, D.; Casado, N.; Sanchez-Sanchez, A.; Malliaras, G. G.; Mecerreyes, D. Conducting Polymer Iongels Based on PEDOT and Guar Gum. ACS Macro Lett. 2017, 6 (4), 473–478. https://doi.org/10.1021/acsmacrolett.7b00104.

(36) del Agua, I.; Marina, S.; Pitsalidis, C.; Mantione, D.; Ferro, M.; Iandolo, D.; SanchezSanchez, A.; Malliaras, G. G.; Owens, R. M.; Mecerreyes, D. Conducting Polymer Scaffolds Based on Poly(3,4-Ethylenedioxythiophene) and Xanthan Gum for Live-Cell Monitoring. ACS Omega 2018, 3 (7), 7424–7431. https://doi.org/10.1021/acsomega.8b00458.

(37) Horikawa, M.; Fujiki, T.; Shirosaki, T.; Ryu, N.; Sakurai, H.; Nagaoka, S.; Ihara, H. The Development of a Highly Conductive PEDOT System by Doping with Partially Crystalline Sulfated Cellulose and Its Electric Conductivity. J. Mater. Chem. C 2015, 3 (34), 8881–8887. https://doi.org/10.1039/C5TC02074C.

(38) Hamedi, M.; Herland, A.; Karlsson, R. H.; Inganäs, O. Electrochemical Devices Made from Conducting Nanowire Networks Self-Assembled from Amyloid Fibrils and Alkoxysulfonate PEDOT. Nano Lett. 2008, 8 (6), 1736–1740. https://doi.org/10.1021/nl0808233.

(39) Xu, Y.; Patsis, P. A.; Hauser, S.; Voigt, D.; Rothe, R.; Günther, M.; Cui, M.; Yang, X.; Wieduwild, R.; Eckert, K.; et al. Cytocompatible, Injectable, and Electroconductive Soft Adhesives with Hybrid Covalent/Noncovalent Dynamic Network. Adv. Sci. 2019, 6 (15), 1802077. https://doi.org/10.1002/advs.201802077.

(40) Xiao, Y.; Li, C. M.; Wang, S.; Shi, J.; Ooi, C. P. Incorporation of Collagen in Poly(3,4Ethylenedioxythiophene) for a Bifunctional Film with High Bio- and Electrochemical Activity. J. Biomed. Mater. Res. Part A 2010, 92A (2), 766–772. https://doi.org/10.1002/jbm.a.32412.

(41) Müller, C.; Jansson, R.; Elfwing, A.; Askarieh, G.; Karlsson, R.; Hamedi, M.; Rising, A.; Johansson, J.; Inganäs, O.; Hedhammar, M. Functionalisation of Recombinant Spider Silk with Conjugated Polyelectrolytes. J. Mater. Chem. 2011, 21 (9), 2909–2915. https://doi.org/10.1039/C0JM03270K.

(42) Singh, B.; Sariciftci, N. S.; Grote, J. G.; Hopkins, F. K. Bio-Organic-SemiconductorField-Effect-Transistor Based on Deoxyribonucleic Acid Gate Dielectric. J. Appl. Phys. 2006, 100 (2), 24514. https://doi.org/10.1063/1.2220488.

(43) Ouyang, J.; Xu, Q.; Chu, C.-W.; Yang, Y.; Li, G.; Shinar, J. On the Mechanism of Conductivity Enhancement in Poly(3,4-Ethylenedioxythiophene):Poly(Styrene Sulfonate) Film through Solvent Treatment. Polymer (Guildf). 2004, 45 (25), 8443–8450. https://doi.org/https://doi.org/10.1016/j.polymer.2004.10.001.

(44) Alemu Mengistie, D.; Wang, P.-C.; Chu, C.-W. Effect of Molecular Weight of Additives on the Conductivity of PEDOT:PSS and Efficiency for ITO-Free Organic Solar Cells. J. Mater. Chem. A 2013, 1 (34), 9907–9915. https://doi.org/10.1039/C3TA11726J.

(45) Yildirim, E.; Wu, G.; Yong, X.; Tan, T. L.; Zhu, Q.; Xu, J.; Ouyang, J.; Wang, J.-S.; Yang, S.-W. A Theoretical Mechanistic Study on Electrical Conductivity Enhancement of DMSO Treated PEDOT:PSS. J. Mater. Chem. C 2018, 6 (19), 5122–5131. https://doi.org/10.1039/C8TC00917A.

(46) Rosu, C.; Kleinhenz, N.; Choi, D.; Tassone, C. J.; Zhang, X.; Park, J. O.; Srinivasarao, M.; Russo, P. S.; Reichmanis, E. Protein-Assisted Assembly of π-Conjugated Polymers. Chem. Mater. 2016, 28 (2), 573–582. https://doi.org/10.1021/acs.chemmater.5b04192.

(47) Eakins, G. L.; Pandey, R.; Wojciechowski, J. P.; Zheng, H. Y.; Webb, J. E. A.; Valéry, C.; Thordarson, P.; Plank, N. O. V; Gerrard, J. A.; Hodgkiss, J. M. Functional Organic Semiconductors Assembled via Natural Aggregating Peptides. Adv. Funct. Mater. 2015, 25 (35), 5640–5649. https://doi.org/10.1002/adfm.201502255.

(48) Demirel, M. C.; Vural, M.; Terrones, M. Composites of Proteins and 2D Nanomaterials. Adv. Funct. Mater. 2017, 28, 1704990. https://doi.org/10.1002/adfm.201704990.

(49) Gaddes, D.; Jung, H.; Pena-Francesch, A.; Dion, G.; Tadigadapa, S.; Dressick, W. J.; Demirel, M. C. Self-Healing Textile: Enzyme Encapsulated Layer-by-Layer Structural Proteins. ACS Appl. Mater. Interfaces 2016, 8 (31), 20371–20378. https://doi.org/10.1021/acsami.6b05232.

(50) Jung, H.; Pena-Francesch, A.; Saadat, A.; Sebastian, A.; Kim, D. H.; Hamilton, R. F.; Albert, I.; Allen, B. D.; Demirel, M. C. Molecular Tandem Repeat Strategy for Elucidating Mechanical Properties of High-Strength Proteins. Proc. Natl. Acad. Sci. 2016, 113 (23), 6478–6483. https://doi.org/10.1073/pnas.1521645113.

(51) Pena-Francesch, A.; Akgun, B.; Miserez, A.; Zhu, W.; Gao, H.; Demirel, M. C. Pressure Sensitive Adhesion of an Elastomeric Protein Complex Extracted From Squid Ring Teeth. Adv. Funct. Mater. 2014, 24 (39), 6227–6233. https://doi.org/10.1002/adfm.201401534.

(52) Pena-Francesch, A.; Domeradzka, N. E.; Jung, H.; Barbu, B.; Vural, M.; Kikuchi, Y.; Allen, B. D.; Demirel, M. C. Research Update: Programmable Tandem Repeat Proteins Inspired by Squid Ring Teeth. APL Mater. 2018, 6 (1), 10701. https://doi.org/10.1063/1.4985755.

(53) Guerette, P. A.; Hoon, S.; Seow, Y.; Raida, M.; Masic, A.; Wong, F. T.; Ho, V. H. B.; Kong, K. W.; Demirel, M. C.; Pena-Francesch, A.; et al. Accelerating the Design of Biomimetic Materials by Integrating RNA-Seq with Proteomics and Materials Science. Nat. Biotechnol. 2013, 31, 908.

(54) Demirel, M. C.; Cetinkaya, M.; Pena-Francesch, A.; Jung, H. Recent Advances in Nanoscale Bioinspired Materials. Macromol. Biosci. 2015, 15 (3), 300–311. https://doi.org/10.1002/mabi.201400324.

(55) Vural, M.; Lei, Y.; Pena-Francesch, A.; Jung, H.; Allen, B.; Terrones, M.; Demirel, M. C. Programmable Molecular Composites of Tandem Proteins with Graphene Oxide for Efficient Bimorph Actuators. Carbon N. Y. 2017, 118, 404–412. https://doi.org/10.1016/j.carbon.2017.03.053.

(56) Vural, M.; Pena-Francesch, A.; Bars-Pomes, J.; Jung, H.; Gudapati, H.; Hatter, C. B.; Allen, B.; Anasori, B.; Ozbolat, I. T.; Gogotsi, Y.; et al. Inkjet Printing of Self-Assembled 2D Titanium Carbide and Protein Electrodes for Stimuli Responsive Electromagnetic Shielding. Adv. Funct. Mater. 2018, 28, 1801972.

(57) Kim, N.; Kee, S.; Lee, S. H.; Lee, B. H.; Kahng, Y. H.; Jo, Y.-R.; Kim, B.-J.; Lee, K. Highly Conductive PEDOT:PSS Nanofibrils Induced by Solution-Processed Crystallization. Adv. Mater. 2014, 26 (14), 2268–2272. https://doi.org/10.1002/adma.201304611.

(58) Sariola, V.; Pena-Francesch, A.; Jung, H.; Çetinkaya, M.; Pacheco, C.; Sitti, M.; Demirel, M. C. Segmented Molecular Design of Self-Healing Proteinaceous Materials. Sci. Rep. 2015, 5, 13482.

(59) Pena-Francesch, A.; Jung, H.; Segad, M.; Colby, R.; Allen, B. D.; Demirel, M. C. MECHANICAL PROPERTIES OF TANDEM REPEAT PROTEINS ARE GOVERNED BY THE NETWORK DEFECTS. ACS Biomater. Sci. Eng. 2018, 4 (3), 884–891. https://doi.org/10.1021/acsbiomaterials.7b00830.

(60) Pena-Francesch, A.; Florez, S.; Jung, H.; Sebastian, A.; Albert, I.; Curtis, W.; Demirel, M. C. Materials Fabrication from Native and Recombinant Thermoplastic Squid Proteins. Adv. Funct. Mater. 2014, 24 (47), 7401–7409. https://doi.org/10.1002/adfm.201401940.

(61) Guerette, P. A.; Hoon, S.; Ding, D.; Amini, S.; Masic, A.; Ravi, V.; Venkatesh, B.; Weaver, J. C.; Miserez, A. Nanoconfined β-Sheets Mechanically Reinforce the SupraBiomolecular Network of Robust Squid Sucker Ring Teeth. ACS Nano 2014, 8 (7), 7170– 7179. https://doi.org/10.1021/nn502149u.

(62) Taroni, P. J.; Santagiuliana, G.; Wan, K.; Calado, P.; Qiu, M.; Zhang, H.; Pugno, N. M.; Palma, M.; Stingelin-Stutzman, N.; Heeney, M.; et al. Toward Stretchable Self-Powered Sensors Based on the Thermoelectric Response of PEDOT:PSS/Polyurethane Blends. Adv. Funct. Mater. 2018, 28 (15), 1704285. https://doi.org/10.1002/adfm.201704285.

(63) Volkov, A. V; Wijeratne, K.; Mitraka, E.; Ail, U.; Zhao, D.; Tybrandt, K.; Andreasen, J. W.; Berggren, M.; Crispin, X.; Zozoulenko, I. V. Understanding the Capacitance of PEDOT:PSS. Adv. Funct. Mater. 2017, 27 (28), 1700329. https://doi.org/10.1002/adfm.201700329.

(64) Ding, D.; Guerette, P. A.; Hoon, S.; Kong, K. W.; Cornvik, T.; Nilsson, M.; Kumar, A.; Lescar, J.; Miserez, A. Biomimetic Production of Silk-Like Recombinant Squid Sucker Ring Teeth Proteins. Biomacromolecules 2014, 15 (9), 3278–3289. https://doi.org/10.1021/bm500670r.

(65) Xia, Y.; Ouyang, J. Significant Different Conductivities of the Two Grades of Poly(3,4Ethylenedioxythiophene):Poly(Styrenesulfonate), Clevios P and Clevios PH1000, Arising from Different Molecular Weights. ACS Appl. Mater. Interfaces 2012, 4 (8), 4131–4140. https://doi.org/10.1021/am300881m.

(66) Raja Ashok, R. P.; Thomas, M. S.; Varughese, S. Multi-Region to Single Region Shear Thinning Transitions in Drying PEDOT:PSS Dispersions: Contributions from Charge Density Fluctuations. Soft Matter 2015, 11 (43), 8441–8451. https://doi.org/10.1039/C5SM01000D.

(67) Gangopadhyay, R.; Das, B.; Molla, M. R. How Does PEDOT Combine with PSS? Insights from Structural Studies. RSC Adv. 2014, 4 (83), 43912–43920. https://doi.org/10.1039/C4RA08666J.

(68) Kim, N.; Lee, B. H.; Choi, D.; Kim, G.; Kim, H.; Kim, J.-R.; Lee, J.; Kahng, Y. H.; Lee, K. Role of Interchain Coupling in the Metallic State of Conducting Polymers. Phys. Rev. Lett. 2012, 109 (10), 106405. https://doi.org/10.1103/PhysRevLett.109.106405.